NUMERICAL ASPECTS OF A BACTERIA GROWTH MODEL

ROBERT STRAKA[*] AND ZDENĚK ČULÍK[†]

Abstract. We numerically investigate the bacteria growth model proposed by Mimura et al. [6]. First the problem and the equations are introduced and the numerical method is described, next several numerical results are presented. Finally the experimental convergence analysis for two different parameter values is indicated, including the experimental order of convergence and L_2, L_∞ distance measured towards the finest mesh.

Key words. reaction-diffusion model, bacterial growth, convergence analysis

AMS subject classifications. 35K57, 65M12, 92B99

1. Introduction. From biological experiments [5], it is known that colonies of *Bacillus Subtilis* perform ability to create various patterns. The shape of such patterns depend on two conditions only, the concentration of nutrient and agar[1]. When these two conditions are varied, one can observe five qualitatively different types of patterns, see Figure 1. C_2 denote concentration of nutrient and C_1 denote diffusion rate in agar. Now when both C_2 and C_1 is low (pattern A - diffusion-limited aggregation-like) we observe dendritic growth, increasing C_2 the branches become thicker and the colony has rough round envelope (pattern B), but when C_1 is increased the colony has a pattern similar to the dense-branching morphology (pattern E). In region C, bacteria actively move and stop when performing cell-division, and repeat this again, the result is concentric ring pattern. Keeping both C_2 and C_1 high, the colony is homogeneously spreading and exhibit the disk-like pattern D. This kind of growth was used for the convergence analysis as will be shown in the second part of this paper.

Reaction–diffusion model. Numerical model proposed by Mimura et al. [6] was used and will be described now. Assume that bacteria consist of two types the active bacteria and the inactive ones. Let $A(t,x,y)$ and $I(t,x,y)$ be their densities respectively and $N(t,x,y)$ the density of nutrients at position (x,y) and time t. Time-evolution is given by the system

$$A_t = \nabla(d_A \nabla A) + \nu g(N)A - a(A,N,I)A + b(A,N,I)I,$$
$$N_t = d_N \Delta N - g(N)A,$$
$$I_t = a(A,N,I)A - b(A,N,I),$$

where d_A is mobility of the active bacteria, d_N is diffusion rate of nutrients, $\nu g(N)$ is the growth rate of bacteria ($\nu > 0$) and $a(A,N,I)$, $b(A,N,I)$ are the conversion functions between the active and the inactive bacteria. We take d_A, d_N as constants for soft agar (i.e. our case, pattern D, agar is soft and nutrients are high). A typical form of growth rate function $g(N)$ would be Michaelis-Menten kinetics [7], $g(N) =$

---

[*]Department of Mathematics, Faculty of Nuclear Sciences and Physical Engineering, Czech Technical University in Prague, Trojanova 13, 120 00, Praha 2, Czech Republic, e-mail: (`straka@kmlinux.fjfi.cvut.cz`)

[†]Department of Mathematics, Faculty of Nuclear Sciences and Physical Engineering, Czech Technical University in Prague, Trojanova 13, 120 00, Praha 2, Czech Republic, e-mail: (`culik@km1.fjfi.cvut.cz`)

[1]Agar is a gelatinous medium used in microbiology to plant bacterial species.
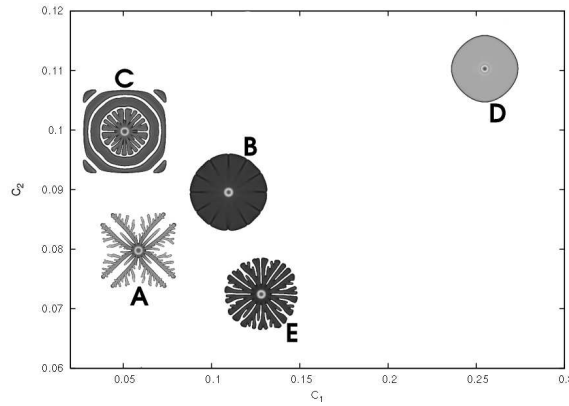
FIG. 1. *Morphological diagram for Bacillus Subtilis.*

$\alpha N/(1 + \beta N)$ with positive α and β. In our computation we use $g(N) = \alpha N$ (the Malthusian growth rate [7]). Essential part of model is specifying the conversion functions $a(A, N, I)$ and $b(A, N, I)$. It is known that bacteria which become inactive, never become active again, unless food is added artificially, so we neglect inactive-active conversion and put $b(A, N, I) \equiv 0$. This reduces our system to

$$
\begin{aligned}
A_t &= d_A \Delta A + \alpha \nu N A - a(A, N)A, \\
N_t &= d_N \Delta N - \alpha N A, \\
I_t &= a(A, N)A.
\end{aligned}
\tag{1}
$$

When the concentration of nutrients become lower, the activity of bacteria become weaker, thus we take that $a(A, N)$ is monotonically decreasing with N and with A, since each bacterium seems to be less active when bacterial populations become sparse. We use continuous form of $a(A, N)$

$$
a(A, N) = \frac{a_0}{(1 + A/a_1)(1 + N/a_2)},
$$

where a_1, a_2 and a_0 are suitable positive constants. Now using dimensional analysis [7]

$$
\begin{aligned}
u &= A, & v &= N, & w &= I, \\
d &= \frac{d_A}{d_N} = C_1, & \alpha &= d_N, & \nu &= 1, \\
t^* &= d_N \cdot t, & a^*(u, v) &= \frac{a(A, N)}{d_N}, & v_0 &= C_2,
\end{aligned}
$$

we obtain from (1) following RD system for the densities of active and inactive bacteria u, w and the concentration of nutrients v (asterisks are dropped for algebraic convenience)

$$
\begin{aligned}
u_t &= d\Delta u + uv - a(u, v)u, \\
v_t &= \Delta v - uv, & x \in \Omega, \quad t > 0, \\
w_t &= a(u, v)u,
\end{aligned}
\tag{2}
$$

where d is ratio of the diffusion rates d_A and d_N. We consider (2) in a two-dimensional bounded domain Ω with initial conditions

$$\begin{aligned}
u(0, x) &= u_0(x) \geq 0, \\
v(0, x) &= v_0, \qquad x \in \Omega, \quad t = 0, \\
w(0, x) &= 0.
\end{aligned}$$

The boundary conditions are

$$\frac{\partial u}{\partial n} = \frac{\partial v}{\partial n} = 0, \qquad x \in \partial\Omega, \quad t > 0,$$

where n is the outward normal vector on $\partial\Omega$. Note that d and v_0 correspond to the parameters C_1 and C_2 respectively (see nondimensionalization).

Discretization of (2). We propose a numerical scheme based on the method of lines with spatially homogeneous finite-difference grid as in [2, 1]. The square domain Ω is covered by an orthogonal mesh ($N + 1 \times N + 1$ nodes) with the equidistant step $h = 1/N$, denoting values of functions u, v, w in nodes (i, j) by the subscripts i, j ($i, j \in 0 \ldots N$). Consequently, we obtain the following system of ODEs:

$$\begin{aligned}
\frac{\mathrm{d}u_{i,j}}{\mathrm{d}t} &= d\frac{u_{i+1,j} + u_{i,j+1} - 4u_{i,j} + u_{i-1,j} + u_{i,j-1}}{h^2} + u_{i,j}v_{i,j} - a(u_{i,j}, v_{i,j})u_{i,j}, \\
(3) \quad \frac{\mathrm{d}v_{i,j}}{\mathrm{d}t} &= \frac{v_{i+1,j} + v_{i,j+1} - 4v_{i,j} + v_{i-1,j} + v_{i,j-1}}{h^2} - u_{i,j}v_{i,j}, \\
\frac{\mathrm{d}w_{i,j}}{\mathrm{d}t} &= a(u_{i,j}, v_{i,j})u_{i,j},
\end{aligned}$$

where $i, j \in 1 \ldots N - 1$ for the first two equations and $i, j \in 0 \ldots N$ for the third equation. The boundary conditions implemented by reflection yield additional equations for the first and second component (e.g. $i = 0$, $j \in 1 \ldots N - 1$) [1]

$$\begin{aligned}
\frac{\mathrm{d}u_{0,j}}{\mathrm{d}t} &= 2d\frac{u_{1,j} - u_{0,j}}{h^2} + d\frac{u_{0,j+1} - 2u_{0,j} + u_{0,j-1}}{h^2} + u_{0,j}v_{0,j} - a(u_{0,j}, v_{0,j})u_{0,j}, \\
\frac{\mathrm{d}v_{0,j}}{\mathrm{d}t} &= 2\frac{v_{1,j} - v_{0,j}}{h^2} + \frac{v_{0,j+1} - 2v_{0,j} + v_{0,j-1}}{h^2} - u_{0,j}v_{0,j},
\end{aligned}$$

and for corners of Ω we have (e.g. $i = 0$, $j = 0$)

$$\begin{aligned}
\frac{\mathrm{d}u_{0,0}}{\mathrm{d}t} &= 2d\frac{u_{1,0} - u_{0,0} + u_{0,1} - u_{0,0}}{h^2} + u_{0,0}v_{0,0} - a(u_{0,0}, v_{0,0})u_{0,0}, \\
\frac{\mathrm{d}v_{0,0}}{\mathrm{d}t} &= 2\frac{v_{1,0} - v_{0,0} + v_{0,1} - v_{0,0}}{h^2} - u_{0,0}v_{0,0}.
\end{aligned}$$

The above obtained system of ODEs is numerically treated by the Merson variant of the Runge-Kutta method with the adaptive time-step control [4, 8]. Besides adaptivity, we observe that such an evolution numerical scheme uses a broad mesh-point stencil to obtain nodal values of the solution at the subsequent time level. This fact can contribute to a successful computation of the numerical solution, namely when studying quantitative aspects of the model.
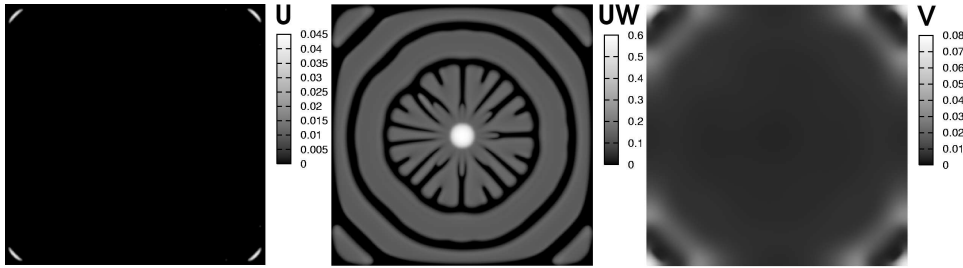
FIG. 2. *Results of numerical simulations for $v_0 = 0.1$, $d = 0.05$, $T = 5775$, concentric ring pattern.*

2. Results of simulations.

2. Results of simulations. Algorithms were implemented in `FORTRAN90` and `C` programming languages, in order to compare accuracy aspects, and compiled with the **Intel Fortran/C Compiler v8.0 for Linux**. Numerical experiments were computed on the computer with `Intel Pentium III (Coppermine) 735MHz` and `Red Hat Linux release 8.0` operating system, partially on `HP-UX C8000` and compiled with `HP Fortran f90 v2.8` and `aCC: HP ANSI C++ B3910B A.03.30` with special care of arithmetical accuracy of the compiled code (by exploring suitable flag setup during compilation). The use of two different programming languages allowed to reduce implementation errors, to verify the same level of accuracy and to competitively compare the CPU usage of both codes. It also opened new computational research items in the given context.

Numerical experiments. Results of numerical experiments are presented in the following figures. In Figures 2 and 3 there are patterns from the regions C and E, in Figures 4 and 5 patterns from the regions A and B and finally Figure 6 shows pattern from the region D. Parameters for the conversion function were set as follows [6]

$$a_0 = 1, \qquad a_1 = \frac{1}{2400}, \qquad a_2 = \frac{1}{120}.$$

Initial condition for the active bacteria was in form

$$u_0(x, y) = 0.4 \exp(-R(x^4 + y^4)),$$

where $R = 10^{-5}$ and additional random noise was added ($\sigma = 0.2$). Number of mesh nodes was $N = 501$ and $\Omega = (-500, 500) \times (-500, 500)$. In each figure, values for d, v_0 and final time T are indicated[2].

Convergence analysis. We have measured convergence of numerically obtained results on several meshes compared to the finest mesh ($N = 2001$) on square domain $\Omega = (-250, 250) \times (-250, 250)$. The results are in following tables and figures, where we have used parameters for disk-like pattern (Table 1, parameters $v_0 = 0.25$, $d = 0.25$, $T = 350$, see also Figure 7) and pattern with round rough envelope (Table 2, parameters $v_0 = 0.09$, $d = 0.15$, $T = 1400$, see also Figure 8). The mesh size h was decreased and L_∞ and L_2 norms were measured. SDoF stands for spatial degree of freedom and the experimental order of convergence (EOC) is the exponent given by the formula (see also [2, 3])

$$\mathrm{Error}_2/\mathrm{Error}_1 = (\mathrm{h}_2/\mathrm{h}_1)^{\mathrm{EOC}}.$$

---

[2]Labels u, uw and v in figures denote densities for active bacteria, active and inactive bacteria and nutrients respectively.
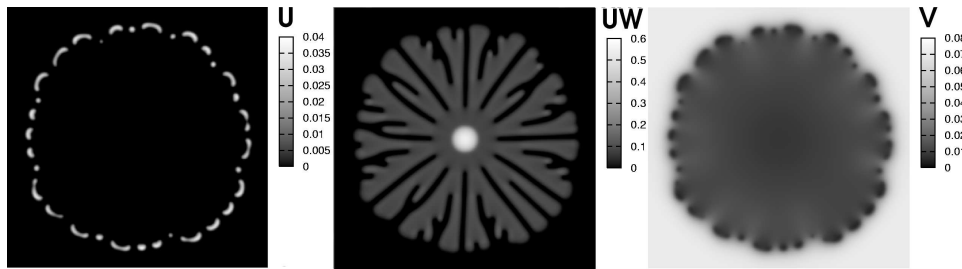
Fig. 3. *Results of numerical simulations for $v_0 = 0.071$, $d = 0.12$, $T = 8600$, dense branch morphology-like pattern.*
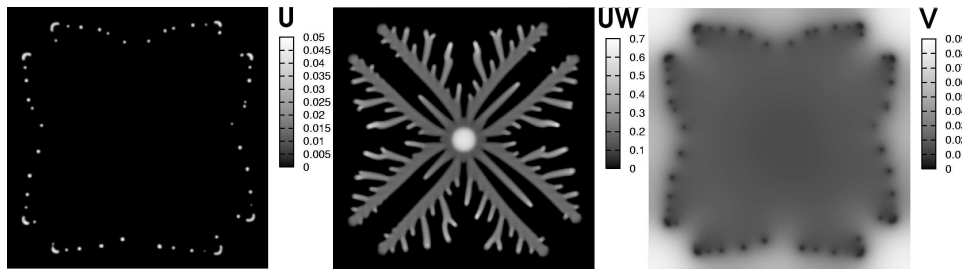

Fig. 4. *Results of numerical simulations for $v_0 = 0.087$, $d = 0.05$, $T = 10000$, diffuse–limited aggregation-like pattern.*
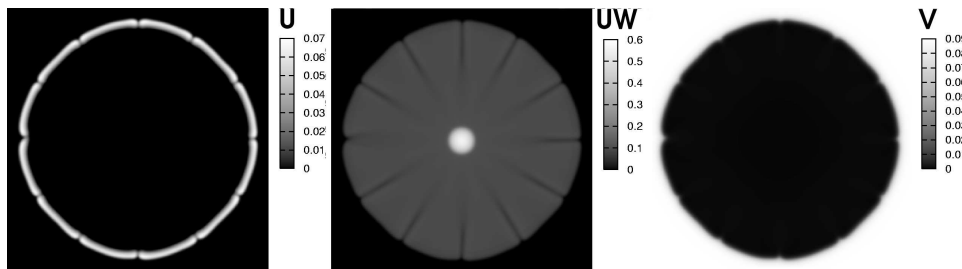

Fig. 5. *Results of numerical simulations for $v_0 = 0.09$, $d = 0.1$, $T = 2485$, pattern with round rough envelope.*
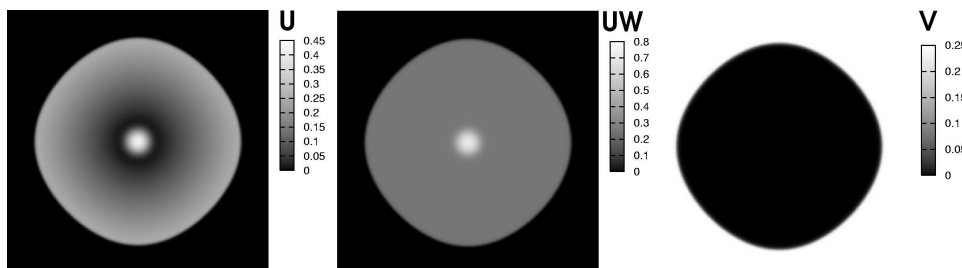

Fig. 6. *Results of numerical simulations for $v_0 = 0.25$, $d = 0.25$, $T = 700$, disk-like pattern.*

3. Conclusion. We present qualitative results for bacteria growth model where five types of patterns were obtained by the numerical simulations with suitable pa-

rameter setting (see Figures 2, 3, 4, 5, 6). We also obtained quantitative results of the pattern growth evaluated by means of measuring numerical convergence (see Tables 1, 2). In Figures 7, 8, we can observe the shape dependence on the mesh size and influence of the orthogonality of the mesh structure. Such asymmetries of patterns vanish as the mesh size h decreases. On the other hand, quantitative behaviour of tree-like and dendritic bacteria patterns obtained by the presented model remain a challenging task for the future.

REFERENCES

[1] M. Beneš, *Diffuse-interface treatment of the anisotropic mean-curvature flow*, Applications of Mathematics, 48 (2003), pp. 437–453.

[2] M. Beneš, *Mathematical and computational aspects of soldification of pure substances*, Acta Mathematica Universitas Comenianae, 70 (2001), pp. 123–151.

[3] G. Dziuk, *Discrete anisotropic curve shortening flow*, SIAM Journal of Numercial Analysis, 36 (1999), pp. 1808–1830

[4] M. Holodniok, A. Klíč, M. Kubíček, M. Marek, *Methods of analysis of nonlinear dynamical models*, (in Czech) Academia, Prague, 1986.

[5] M. Matsushita, J. Wakita, H. Itoh, K. Watanabe, T. Arai, T. Matsuyama, H. Sakaguchi, M. Mimura, *Formation of colony patterns by a bacterial cell population*, Physica A, 274 (1999), pp. 190–199.

[6] M. Mimura, H. Sakaguchi, M. Matsushita, *Reaction–diffusion modelling of bacterial colony patterns*, Physica A, 282 (2000), pp. 283–303.

[7] J.D. Murray, *Mathematical Biology*, Springer-Verlag, Berlin Heidelberg, 1993.

[8] R. Straka, *Numerical algorithms for investigation chaotic dynamics of reaction–diffusion equations*, diploma thesis (in Czech), Prague, 2004.

Mesh h	SDoF $N*N$	$\mathcal{L}_\infty(0,T;\mathcal{L}_2)$ error of u	$\mathcal{L}_\infty(0,T;\mathcal{L}_\infty)$ error of u	EOC u L_2	EOC u L_∞
2.0	63001	24.67872	0.23843	–	–
1.667	90601	19.74641	0.22235	1.22429	0.3834
1.25	160801	12.85131	0.17905	1.49202	0.75221
1.0	251001	8.74512	0.13481	1.72512	1.27192
0.833	361201	6.28791	0.09921	1.80529	1.67806
0.713	491401	4.82112	0.08012	1.70761	1.37389
0.625	641601	3.55618	0.06070	2.28885	2.10691
0.556	811801	2.79808	0.04724	2.07349	2.14347
0.5	1002001	2.27929	0.04008	1.93169	1.54761
0.455	1212201	1.79743	0.03153	2.51836	2.54438
0.417	1442401	1.52109	0.02700	1.91399	1.77767
0.385	1692601	1.22657	0.02218	2.69544	2.46551

Mesh h	SDoF $N*N$	$\mathcal{L}_\infty(0,T;\mathcal{L}_2)$ error of v	$\mathcal{L}_\infty(0,T;\mathcal{L}_\infty)$ error of v	EOC v L_2	EOC v L_∞
2.0	63001	24.10103	0.23318	–	–
1.667	90601	19.09298	0.21265	1.279	0.50588
1.25	160801	12.26536	0.16641	1.53723	0.85188
1.0	251001	8.29076	0.12326	1.75509	1.34495
0.833	361201	5.94117	0.09006	1.82373	1.71749
0.713	491401	4.54911	0.07256	1.71631	1.38901
0.625	641601	3.36055	0.05481	2.29885	2.12933
0.556	811801	2.63529	0.04257	2.07816	2.16146
0.5	1002001	2.14644	0.03615	1.93277	1.53854
0.455	1212201	1.69201	0.02840	2.52248	2.55885
0.417	1442401	1.43216	0.02436	1.91177	1.75932
0.385	1692601	1.15457	0.01998	2.69853	2.48273

Mesh h	SDoF $N*N$	$\mathcal{L}_\infty(0,T;\mathcal{L}_2)$ error of w	$\mathcal{L}_\infty(0,T;\mathcal{L}_\infty)$ error of w	EOC w L_2	EOC w L_∞
2.0	63001	2.34153	0.01379	–	–
1.667	90601	1.76969	0.01046	1.53742	1.51628
1.25	160801	1.08381	0.00683	1.7032	1.47952
1.0	251001	0.71987	0.00465	1.83366	1.72084
0.833	361201	0.51403	0.00326	1.84322	1.94448
0.713	491401	0.40059	0.00261	1.60293	1.43949
0.625	641601	0.29514	0.00195	2.31911	2.22018
0.556	811801	0.23341	0.00151	2.00578	2.17304
0.5	1002001	0.19417	0.00128	1.73395	1.53584
0.455	1212201	0.15418	0.00101	2.44512	2.55881
0.417	1442401	0.13354	0.00087	1.64788	1.74227
0.385	1692601	0.10929	0.00071	2.51017	2.43099

TABLE 1

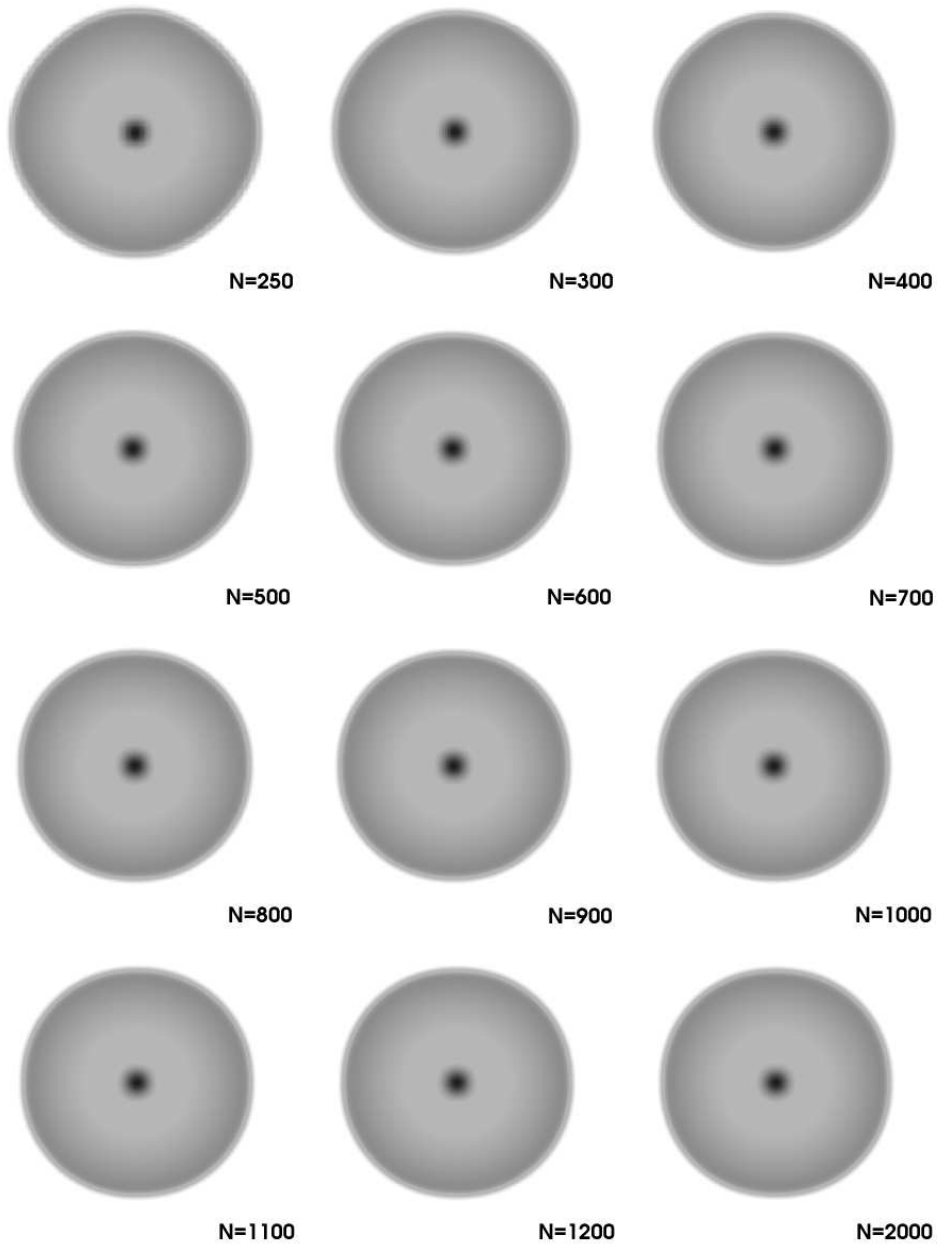*Table of convergence errors and EOC coefficients for disk-like pattern.*

FIG. 7. *Results of numerical simulations for $v_0 = 0.25$, $d = 0.25$, $T = 700$ and different mesh size N, compound u for disk-like pattern.*
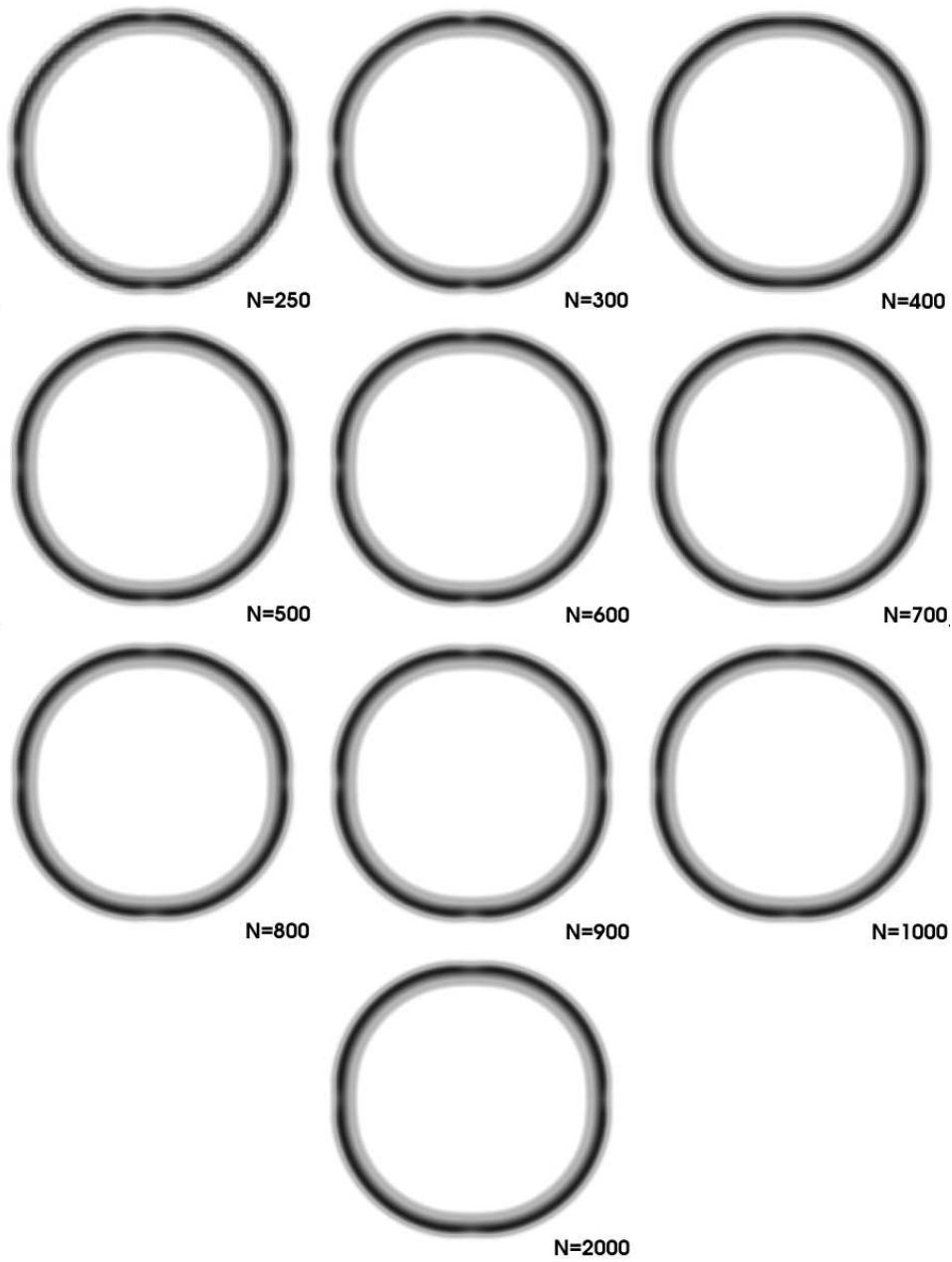
FIG. 8. *Results of numerical simulations for $v_0 = 0.09$, $d = 0.15$, $T = 1400$ and different mesh size N, compound u for pattern with round rought envelope.*

Mesh h	SDoF N*N	$\mathcal{L}_\infty(0,T;\mathcal{L}_2)$ error of u	$\mathcal{L}_\infty(0,T;\mathcal{L}_\infty)$ error of u	EOC u L_2	EOC u L_∞
2.0	63001	4.10622	0.05021	–	–
1.667	90601	3.07952	0.04006	1.57989	1.23953
1.25	160801	1.78246	0.02722	1.89931	1.34231
1.0	251001	1.22904	0.01743	1.66601	1.99675
0.833	361201	0.95551	0.01386	1.37776	1.25506
0.713	491401	0.74504	0.01074	1.59955	1.63918
0.625	641601	0.53725	0.00854	2.48208	1.74240
0.556	811801	0.52373	0.00783	0.21784	0.73648
0.5	1002001	0.41752	0.00567	2.13505	3.04800

Mesh h	SDoF N*N	$\mathcal{L}_\infty(0,T;\mathcal{L}_2)$ error of v	$\mathcal{L}_\infty(0,T;\mathcal{L}_\infty)$ error of v	EOC v L_2	EOC v L_∞
2.0	63001	3.49169	0.04199	–	–
1.667	90601	2.58035	0.03211	1.66077	1.47328
1.25	160801	1.47564	0.02119	1.94119	1.44426
1.0	251001	1.01498	0.01366	1.67707	1.96787
0.833	361201	0.78628	0.01076	1.39724	1.30663
0.713	491401	0.61315	0.00843	1.59884	1.56386
0.625	641601	0.44198	0.00663	2.48501	1.82121
0.556	811801	0.42842	0.00603	0.26637	0.81518
0.5	1002001	0.34343	0.00449	2.08276	2.78712

Mesh h	SDoF N*N	$\mathcal{L}_\infty(0,T;\mathcal{L}_2)$ error of w	$\mathcal{L}_\infty(0,T;\mathcal{L}_\infty)$ error of w	EOC w L_2	EOC w L_∞
2.0	63001	2.84203	0.02392	–	–
1.667	90601	2.12037	0.01970	1.6084220	1.0667881
1.25	160801	1.26813	0.01414	1.7856134	1.1518897
1.0	251001	0.89162	0.01095	1.5786252	1.1470427
0.833	361201	0.69800	0.00907	1.3398770	1.0311038
0.713	491401	0.55540	0.00757	1.4691713	1.1576636
0.625	641601	0.40751	0.00634	2.3504215	1.3539341
0.556	811801	0.39702	0.00559	0.2229633	1.0751357
0.5	1002001	0.32255	0.00481	1.9565191	1.4166847

TABLE 2

Table of convergence errors and EOC coefficient for pattern with round rough envelope.